

Asymmetric distribution of pathogenic low wall shear stress of the bilateral subclavian arteries: two case reports

Journal of International Medical Research
49(9) 1–11

© The Author(s) 2021

Article reuse guidelines:

sagepub.com/journals-permissions

DOI: 10.1177/03000605211042503

journals.sagepub.com/home/imr



Huai Wu Yuan¹ , Jin Xun Yao², Si Yu Huang³,
Min Yong Cui⁴, Ren Jie Ji¹, Jia Rui Li¹ and
Li Hua Chen²

Abstract

The effects of increasing blood flow on the pathogenic wall shear stress (pWSS) of subclavian arteries (SAs) are currently unclear. Patient-specific models of the SA were constructed based on computed tomographic images from two patients. Using the Ansys Fluent 19.0 transient laminar flow solver, the finite volume method was chosen to solve the Navier–Stokes equation governing fluid behavior. The time-averaged wall shear stress, ratio of risk area, cumulative ratio of risk area (\bar{P}), ratio of risk time, and ratio contour of risk time were calculated to describe the temporal and spatial distributions of pWSS. Virtually all pWSS occurred during the diastolic phase. The \bar{P} was 2.3 and 1.29 times higher on the left than on the right in Patients 1 (P1) and 2 (P2), respectively. Increasing the blood flow volume of the left SA by 20%, 40%, and 60% led to a 9.27%, 15.10%, and 20.99% decrease in \bar{P} for P1 and a 5.74%, 11.55%, and 17.14% decrease in \bar{P} for P2, respectively, compared with baseline values. In conclusion, the left SA showed greater diastolic pWSS than the right SA, and increasing the blood flow volume reduced the pWSS in the left SA.

¹Department of Neurology, the First Affiliated Hospital, College of Medicine, Zhejiang University, Hangzhou, Zhejiang Province, China

²College of Aeronautics and Astronautics, Zhejiang University, Hangzhou, Zhejiang Province, China

³Department of Neurology, Shengzhou People's Hospital, Shengzhou, Zhejiang Province, China

⁴Department of Ultrasonography, the First Affiliated Hospital, College of Medicine, Zhejiang University, Hangzhou, Zhejiang Province, China

Corresponding author:

Huai Wu Yuan, Department of Neurology, the First Affiliated Hospital, College of Medicine, Zhejiang University, 79 Qingchun Road, Hangzhou, Zhejiang Province 310003, China.

Email: 1313007@zju.edu.cn



Creative Commons Non Commercial CC BY-NC: This article is distributed under the terms of the Creative

Commons Attribution-NonCommercial 4.0 License (<https://creativecommons.org/licenses/by-nc/4.0/>) which permits non-commercial use, reproduction and distribution of the work without further permission provided the original work is attributed as specified on the SAGE and Open Access pages (<https://us.sagepub.com/en-us/nam/open-access-at-sage>).

Keywords

Subclavian artery, wall shear stress, ratio of risk area, ratio of risk time, case report, stenosis, atherosclerosis

Date received: 5 March 2021; accepted: 10 August 2021

Introduction

Stenosis of the subclavian artery (SA) may lead to symptoms that indicate ischemia of the posterior intracranial circulation and upper limbs, such as subclavian steal syndrome. SA stenosis is diagnosed when there is a blood pressure difference ≥ 15 mmHg between the bilateral brachial arteries.¹ In a previous study, patients with a bilateral blood pressure difference ≥ 15 mmHg had a 60% and 70% higher risk of cardiovascular and all-cause mortality, respectively, compared with the general population.² Atherosclerosis is the most common cause of SA stenosis; other causes, such as inflammation and dissection, account for $<10\%$ of all cases.³ SA stenosis occurs on the left side in most cases,^{3,4} thus contributing to asymmetry. The prevention of atherosclerotic plaques in the left SA is therefore essential for preventing SA stenosis.

Wall shear stress (WSS) is the force per unit area caused by a moving fluid in the local tangent of a luminal surface. Biomechanical studies have revealed that arterial walls that possess a WSS <0.4 Pa are prone to the formation of atherosclerotic plaques.⁵ Furthermore, there are clear differences between the bilateral SAs in terms of their distance from the heart and their three-dimensional (3D) morphology. These factors may have an impact on the distribution of pathogenic WSS (pWSS).⁶ In addition, the bilateral arteries are affected by the same risk factors as for atherosclerosis, such as hypertension, hyperlipidemia, diabetes, and smoking. We therefore speculate that differences in

pWSS may cause an asymmetric incidence of SA stenosis between the bilateral SAs, and that pWSS may be an important target for the prevention of atherosclerotic plaques in the left SA.

To the best of our knowledge, previous studies focusing on the SA have primarily reported that right SA cannulation may be cerebroprotective against the formation of ascending aortic plaques, and that the right SA is a feasible anastomosis location for left ventricular assist devices (standard treatment options for end-stage heart failure patients).^{7,8} No studies have directly reported on the asymmetric distribution of pWSS of the bilateral SAs, which may be a potential therapeutic target for the prevention of SA stenosis. The present study aimed to describe both the asymmetric pWSS distribution of the bilateral SAs and the effects of increasing blood flow on the pWSS of the left SA.

Case reports

Two patients were consecutively admitted to the Department of Neurology in February 2019 and underwent computed tomography angiography and ultrasonography of the bilateral SAs. Both patients were older men with dizziness but no abnormal neurological signs. They both had a history of hypertension and anti-hypertensive drugs. In addition, both were diagnosed with cerebral atherosclerosis and received antiplatelet drugs (100 mg aspirin orally once per day) for primary stroke prevention. This study followed the ethical

guidelines of the 1975 Declaration of Helsinki. It was approved by the Ethics Committee of the First Affiliated Hospital of the College of Medicine of Zhejiang University (reference number 2018-591), and verbal consent for treatment was obtained from the patients or their legally authorized representatives. All patient details have been de-identified. The reporting of this study conforms to the CARE guidelines (for CAse REports).⁹

Methods

Three-dimensional modeling

Mimics software (Materialise's Interactive Medical Image Control System; Materialise, Leuven, Belgium) was used to extract 3D vascular morphology from each raw computed tomography angiography image; the SA segment from its origin to the vertebral artery ostium was selected. The vascular morphology of the bilateral SAs was established via the following steps: (1) the Dynamic Growing function of Mimics software was used to acquire the initial vascular geometry; (2) blood vessels that were not within the region of interest (ROI) were deleted and only the SA ROI was retained; (3) each pixel on the arterial section was reviewed individually and adjusted manually; and (4) smoothing was performed on the vascular geometry (Figure 1a–c and i–k). The bilateral ROI was defined as the area between the SA origin and vertebral artery ostium.

Meshing

The process of meshing was performed using Ansys Mesh, which is part of the solver package of Ansys Workbench (Ansys Inc., Canonsburg, PA, USA). Unstructured tetrahedral grids were used, and the surface grid size of the core area was 0.1 mm. Ten prism layers were adopted

to accurately capture boundary phenomena in blood flow, and the height of the first layer was 0.01 mm with a growth rate of 1.2. The mesh in the key region was between two and three million (Figure 1d, e, l, and m). The independence of the mesh was calculated to ensure the results were limited to 1%.

Boundary conditions

To ensure full development of the SA flow, the inlet (10 times the diameter) and outlet (20 times the diameter) boundaries were extended as appropriate. The blood flow velocity was extracted from the blood flow spectrum measured using ultrasonography, and piecewise polynomial fitting was performed to obtain the dynamic curve of outlet blood flow velocity. Next, the inlet velocity–time curve was created according to the scaling principle (Figure 1f–h and n–p). Velocity was inputted as a boundary condition through a Fluent User-Defined Function.

We assumed that there was a no-slip boundary, rigid wall, velocity inlet boundary, and pressure outlet boundary, and we set the pressure to 0 (the SA outlet was used as the reference pressure of 0).

Blood is considered an incompressible non-Newtonian fluid, with a density of 1060 kg/m³. A Carreau fluid is an intuitive shear-thinning fluid that conforms to the shear thinning of blood.¹⁰ The specific parameters were as follows:

$$\mu = \mu_0 + (\mu_0 - \mu_\infty)(1 + A|\dot{\gamma}|2)^n \quad (1)$$

where μ is the blood flow viscosity, $A = 10.976$, $n = -0.3216$, $\mu_\infty = 0.0035$, and $\mu_0 = 0.056$.

Hemodynamic analysis

A finite volume laminar flow solver package, Ansys Fluent 19.0 (Ansys Inc.), was

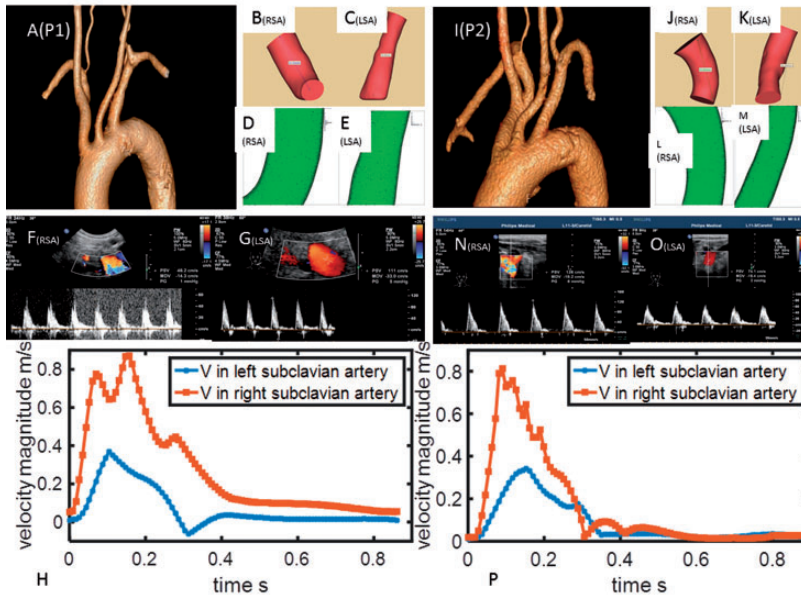


Figure 1. Three-dimensional (3D) model and mesh generation before fluid dynamics calculation. (a) computed tomography angiography (CTA) of the subclavian artery (SA) of Patient 1 (P1); (b) 3D modeling of the right subclavian artery (RSA) of P1; (c) 3D modeling of the left subclavian artery (LSA) of P1; (d) meshing of the RSA of P1; (e) meshing of the LSA of P1; (f) ultrasonography of the RSA of P1; (g) ultrasonography of the LSA of P1; (h) the inlet velocity (V)–time curve of the SA of P1; (i) CTA of the SA of Patient 2 (P2); (j) 3D modeling of the RSA of P2; (k) 3D modeling of the LSA of P2; (l) meshing of the RSA of P2; (m) meshing of the LSA of P2; (n) ultrasonography of the RSA of P2; (o) ultrasonography of the LSA of P2; (p) the inlet V–time curve of the SA of P2.

selected to solve the Navier–Stokes equation that governs 3D incompressible fluids. The time step was set at 1/400 of the cardiac cycle, and the convergence criterion of the iterative residual was 10^{-5} . To ensure the convergence of the solution, the overall result was calculated according to the cycle and time step until the data had <3% error.

The Navier–Stokes equation:

$$\nabla \cdot \mathbf{u} = 0, \quad \frac{\partial \mathbf{u}}{\partial t} + \mathbf{u} \cdot \nabla \mathbf{u} = -\nabla p + \nu \Delta \mathbf{u}, \quad (2)$$

where \mathbf{u} is the velocity, μ is the viscosity of blood, and $\nu = \mu/\rho$ is the ratio of blood flow viscosity to density (known as the kinematic viscosity).

WSS was related to the velocity profile near the wall:

$$\text{WSS} = \mu \left. \frac{\partial u_t}{\partial n} \right|_{\text{wall}} \quad (3)$$

The viscosity follows Equation (1). WSS was defined as the normal velocity gradient at the wall, which is equal to the product of viscosity. Viscosity is dependent on stress and the gradient of the velocity at the wall, u_t is the tangential velocity, and n is the unit vector normal to the wall. WSS during a cardiac cycle was integrated using the time-averaged wall shear stress (TAWSS) and oscillatory shear index (OSI).

The TAWSS was calculated to describe the temporal distribution of instantaneous pWSS within one cycle. The transient WSS

of each grid cell was averaged over time to obtain its TAWSS distribution. The TAWSS of each grid cell was then weighted and averaged according to the grid cell area to obtain the final TAWSS of the overall arterial wall.

$$\text{TAWSS} = \frac{1}{T} \int_0^T |\text{WSS}| dt \quad (4)$$

OSI is another vital parameter for the risk of atherosclerosis, and indicates the WSS vibration during a cardiac cycle.

$$\text{OSI} = 0.5 \left(1 - \frac{|\int_0^T \text{WSS} dt|}{\int_0^T |\text{WSS}| dt} \right) \quad (5)$$

The ratio of risk area (P_{risk}) and cumulative ratio of risk area (\bar{P}) were calculated to describe the temporal distribution of shear stress. pWSS was defined as a WSS or TAWSS value $< 0.4 \text{ Pa}$. P_{risk} was defined as the relative size of the arterial wall area where pWSS was present at each timepoint. \bar{P} was defined as the relative size of the arterial wall area where pWSS was present in each cardiac cycle, which was determined by calculating the integral of P_{risk} at time t (i.e., the area under the P_{risk} [y-axis] – time [x-axis] curve).

$$P_{risk}(t) = \frac{S_{<0.4Pa}(t)}{S(t)} \quad (6)$$

$$\bar{P} = \int_0^T P_{risk}(t) dt, \quad (7)$$

where s is the area of the arterial wall.

The ratio of risk time was calculated. Additionally, the contour of the ratio of risk time was plotted to illustrate the spatial distribution of pWSS, to identify the arterial wall regions with the greatest risk of atherosclerosis.¹¹ The ratio of risk time was

defined as the percentage of time in which pWSS occurred at each calculating mesh node on the arterial wall surface across the entire cycle. If any location had a ratio of risk time of 100%, then pWSS was considered present at that node throughout the entire cycle.

Intervention

The equation for WSS suggests that WSS increases with increasing blood flow volume. To test the hypothesis that a higher blood flow volume can reduce pWSS, we calculated P_{risk} , \bar{P} , ratio of risk time, and its contour for the left SA after increasing the blood flow by 20%, 40%, and 60%.

Results

Asymmetric distribution of pWSS in the bilateral SAs

The TAWSS contour crudely showed that the WSS of the left SA was lower than that of the right SA (Figures 2 and 3). Patient 1 (P1) had low WSS at the left SA inlet (Figure 2a, b), whereas Patient 2 (P2) had low WSS in the midsection of the left SA (Figure 3a, b). Furthermore, the P_{risk} –time curve accurately revealed the differences in pWSS distribution. Both P1 (Figure 4a–c) and P2 (Figure 4d–f) had greater pWSS in the left SA than in the right SA, and virtually all pWSS occurred during the diastolic phase. Furthermore, \bar{P} quantitatively demonstrated the difference in pWSS between the bilateral SAs. The \bar{P} values of the left and right SAs in P1 were 0.6052 and 0.2603, respectively; the \bar{P} of the left SA was 2.3 times higher than that of the right SA. For P2, the \bar{P} values of the left and right SAs were 0.6128 and 0.4731, respectively; the left SA was 1.29 times higher than that of the right SA.

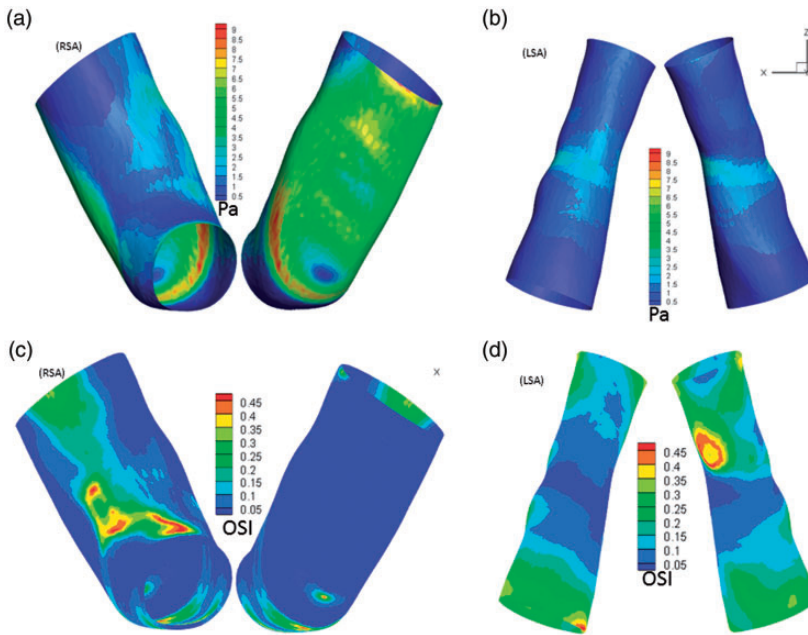


Figure 2. Contours of the time-averaged wall shear stress (TWSS) and oscillatory shear index (OSI) of Patient I (P1). (a) TWSS on the ventral and dorsal sides of the right subclavian artery (RSA); (b) TWSS on the ventral and dorsal sides of the left subclavian artery (LSA); (c) OSI on the ventral and dorsal sides of the RSA; (d) OSI on the ventral and dorsal sides of the LSA.

The high OSIs in the left and right SAs were usually matched with low WSS, while the region of high OSI in the right SA was a little bigger than the one of low WSS (Figure 2c, d; Figure 3c, d). The more severe direction change of the WSS in the right SA may be caused by the high change rate of transient velocity.

In addition, the contour of the ratio of risk time revealed the arterial wall areas with the greatest risk of atherosclerosis; that is, the areas with the longest pWSS duration. Because of the higher incidence of SA stenosis on the left side than the right side, we focused mainly on the left SA. The ratio contour of risk time indicated that P1 had the greatest risk at the left SA inlet (Figure 4c), while P2 had the greatest risk at the proximal end of the dorsal mid-section of the left SA (Figure 4f).

Effects of increasing local blood flow on pWSS of the left SA

Because there was a higher incidence of left SA stenosis than right SA stenosis, we mainly focused on the left SA. Compared with baseline (\bar{P} [0.6052]), increasing the blood flow by 20%, 40%, and 60% led to a decrease in \bar{P} of the left SA by 9.27%, 15.10%, and 20.99% (to 0.549127, 0.513504, and 0.478164), respectively, in P1 (Figure 5a). In P2, whose baseline \bar{P} was 0.6128, increasing the blood flow by 20%, 40%, and 60% led to a decrease in \bar{P} of the left SA by 5.74%, 11.55%, and 17.14% (to 0.57747, 0.542020, and 0.507669), respectively (Figure 6a). pWSS mainly occurred during the diastolic phase. The contour of the ratio of risk time showed that the greatest risk area

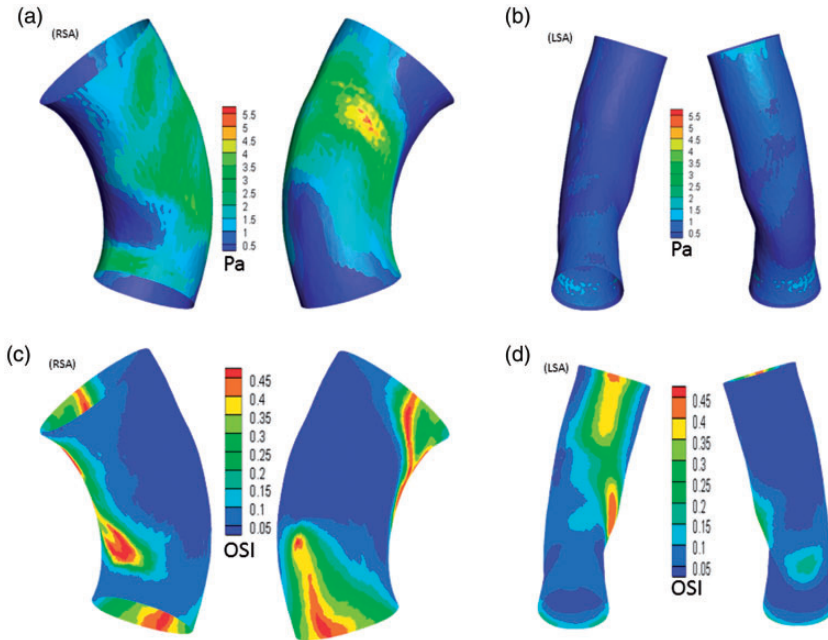


Figure 3. Contours of the time-averaged wall shear stress (TWSS) and oscillatory shear index (OSI) of patient 2 (P2). (a) TWSS on the ventral and dorsal sides of the right subclavian artery (RSA); (b) TWSS on the ventral and dorsal sides of the left subclavian artery (LSA); (c) OSI on the ventral and dorsal sides of the RSA; (d) OSI on the ventral and dorsal sides of the LSA.

was still at the inlet for P1 (Figure 5b–d) and in the dorsal and ventral midsection for P2 (Figure 6b–d), but the range was reduced.

Discussion

In the present study, we revealed that the left SA had significantly greater pWSS during the diastolic phase than the right SA, while its \bar{P} was approximately 1.3 to 2.3 times higher than that of the right SA. The equation for shear stress demonstrated that WSS was positively correlated with blood flow. Because the left SA is farther from the heart, its flow velocity is slower than that of the right SA. This was reflected in the inlet velocity–time curves of the two patients included in our study (Figure 1h, p), and meant that the pWSS in the left SA was higher than that in the right SA. In

addition, curved arteries generally have higher shear stress than straight segments.⁶ Because the natural structure of the right SA is more curved than that of the left SA (Figure 1a–c and i–k), the right SA has higher shear stress than the left SA. High resistance causes a sharp decline in blood flow velocity in the extracranial arteries to near baseline in the early diastole, while regurgitation is common in the late diastole (Figure 1f, g, n, and o). Furthermore, because the heart only ejects blood during systole, the velocity of blood flow in human arteries is always lower during diastole than during systole, which means that all pWSS in the bilateral SAs occurs during the diastolic phase.

This pWSS asymmetry between the bilateral SAs is consistent with the asymmetrical incidence of SA stenosis that is observed by clinicians; that is, the left SA is more

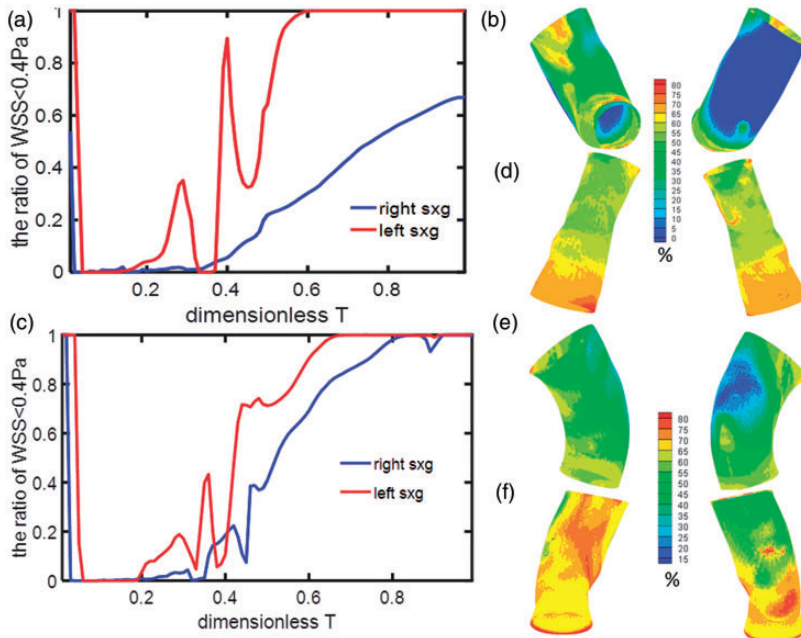


Figure 4. The temporal and spatial distributions of pathogenic wall shear stress (pWSS). (a) ratio of risk area (P_{risk})–time (T) curve of the bilateral subclavian artery of Patient 1 (P1); (b) contour of the ratio of risk time of the right subclavian artery (RSA) of P1; (c) contour of the ratio of risk time of the left subclavian artery (LSA) of P1; (d) P_{risk} –T curve of the bilateral subclavian arteries of Patient 2 (P2); (e) contour of the ratio of risk time of the RSA of P2; (f) contour of the ratio of risk time of the LSA of P2.

susceptible to atherosclerotic stenosis. In recent decades, research in the field of biomechanics has confirmed that pWSS (<0.4 Pa) plays a crucial role in the pathogenesis and rupture of atherosclerosis.¹² Given that the bilateral SAs share the same risk factors (e.g., hypertension), arterial wall tissue components, and intraluminal blood components, it can be inferred that the asymmetry of shear stress is an important cause of the asymmetric incidence of SA atherosclerotic stenosis. A similar relationship has also been reported in a comparative study of the bilateral coronary arteries.¹³ pWSS can inhibit a series of anti-atherosclerotic functions of arterial endothelial cells, such as nitric oxide synthesis and antioxidant activity. It also enhances a series of pro-atherosclerotic factors, such as the secretion of inflammatory and

growth factors.⁵ Therefore, the first clinical implication of our study is that pWSS may be a key target in the prevention of SA atherosclerosis.

With respect to the pWSS asymmetry of the bilateral SAs, our findings revealed that increasing blood flow can decrease the duration of pWSS in the left SA with no migration in areas at greatest risk of atherosclerosis. Thus, this intervention can theoretically reduce the risk of atherosclerotic stenosis in the left SA. Based on its definition, WSS is associated with the derivative of wall velocity. Because WSS increases with increased central blood flow velocity under no-slip boundary conditions, we can deduce that pWSS decreases with increasing flow and that minimal change occurs in the position with the most obvious pWSS under laminar flow. Limb movement is

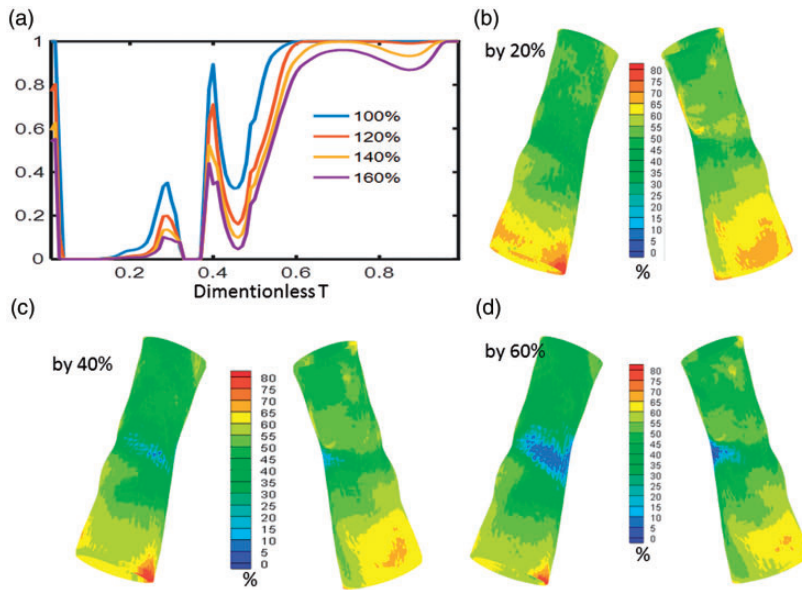


Figure 5. Effects of increasing local blood flow on the pathogenic wall shear stress (pWSS) of the left subclavian artery (LSA) of Patient 1 (P1). (a) ratio of risk area (P_{risk})–time (T) curve of the LSA; (b–d) contours of the ratio of risk time of the LSA when increasing the blood flow by 20%, 40%, and 60%, respectively.

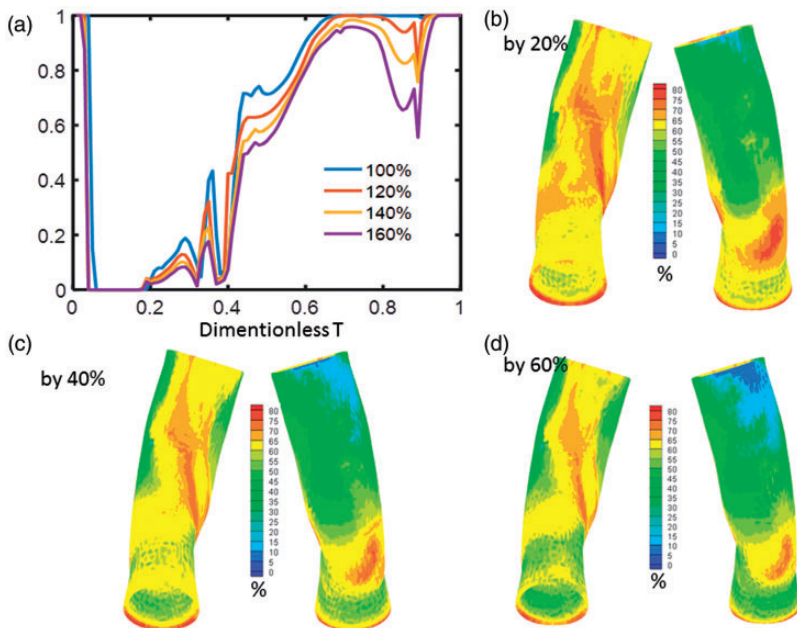


Figure 6. Effects of increasing local blood flow on the pathogenic wall shear stress (pWSS) of the left subclavian artery (LSA) of Patient 2 (P2). (a) ratio of risk area (P_{risk})–time curve of the LSA; (b–d) contours of the ratio of risk time of the LSA when increasing the blood flow by 20%, 40%, and 60%, respectively.

generally accompanied by an increase in local arterial blood flow, thus further increasing arterial WSS and reducing pWSS. Exercise prevents atherosclerosis not only by increasing shear stress to promote the transformation of endothelial cell function, but also by releasing anti-inflammatory factors through muscle contraction.¹⁴ It is therefore necessary to further investigate the pWSS range of the left SA in the general population and to examine whether left upper limb movements that increase blood flow in the left SA can prevent its stenosis.

The second implication of our study involves the new index, the “cumulative ratio of risk area” (\bar{P}). This was used to describe the temporal distribution of pWSS. Considering the normal distribution of WSS in the population, patients who are prone to SA atherosclerosis comprise only a small proportion of the general population. If the groups at greatest risk need to be defined, it may be more reasonable to use \bar{P} instead of WSS size alone. Of course, this needs to be confirmed by rigorous cohort studies, and we will explore the accuracy of \bar{P} as a marker of risk groups in subsequent studies.

The limitations of the present study are as follows. (1) Ultrasonography was unable to measure the finer velocity distribution of blood vessel sections; we were therefore unable to obtain more accurate data on blood flow. In the current study, we incorporated the theoretical velocity distribution patterns of a cylindrical section and calculated the blood flow according to the maximum velocity measured at the section. (2) The present study assumed that the arterial wall is a rigid structure and ignored the fact that it is an elastic tissue. However, because this was a bilateral comparison, assuming that the arterial wall is a rigid structure did not affect the differences in the distribution of pWSS bilaterally. (3) Partial corrections should be considered for the outlet

pressure, such as the addition of autonomous regulation and other correction terms, to adapt to the changes in blood flow.⁸ Numerical simulation should also be performed using medically related Windkessel models.¹⁵ (4) There are certain WSS processing methods, such as the WSS temporal gradient, that can be used to describe the changes in WSS under different cycle conditions.¹⁶ (5) No clinical cohort study on SA has verified the causal relationship between pWSS and the risk of atherosclerosis. However, previous studies have confirmed the causal relationship between pWSS and the site and size of atherosclerotic plaques and relative risk.¹² (6) Factors such as age, heart rhythm, blood pressure, and aortic arch type may affect WSS. Hence, it is necessary to expand the sample size and devote more computing resources to studying pWSS distribution of the bilateral SAs under differing pathophysiological conditions. This will enable us to obtain detailed evidence for determining the pWSS characteristics of patients at high risk for SA stenosis, thereby providing a clear target pWSS range for further interventional studies. (7) Our computational model was based on pressure-driven flow, and it was the pressure that led to our results. Although we acknowledge that the physiological components that influence real blood flow are intricate and complex, we have put forward a simplified model to show the tendencies of SA flow. All of the aforementioned limitations will be considered in our future work.

In conclusion, the left SA showed greater diastolic pWSS than the right SA, and increasing blood flow volume reduced the pWSS in the left SA. It is necessary to further investigate the pWSS range of the left SA in the general population, and to examine and confirm whether precise upper limb movements that increase the blood flow volume of the left SA can prevent stenosis.

Declaration of conflicting interest

The authors declare that there is no conflict of interest.

Funding

The authors disclosed receipt of the following financial support for the research, authorship, and/or publication of this article: This work was supported by the Natural Science Foundation of Zhejiang Province (grant number LSY19H020001).

ORCID iD

Huai Wu Yuan  <https://orcid.org/0000-0002-8066-4477>

References

1. Aboyans V, Criqui MH, McDermott MM, et al. The vital prognosis of subclavian stenosis. *J Am Coll Cardiol* 2007; 49: 1540–1545.
2. Clark CE, Taylor RS, Shore AC, et al. Association of a difference in systolic blood pressure between arms with vascular disease and mortality: a systematic review and meta-analysis. *Lancet* 2012; 379: 905–914.
3. Ackermann H, Diener HC and Dichgans J. Stenosis and occlusion of the subclavian artery: ultrasonographic and clinical findings. *J Neurol* 1987; 234: 396–400.
4. Labropoulos N, Nandivada P and Bekelis K. Prevalence and impact of the subclavian steal syndrome. *Ann Surg* 2010; 252: 166–170.
5. Malek AM, Alper SL and Izumo S. Hemodynamic shear stress and its role in atherosclerosis. *JAMA* 1999; 282: 2035–2042.
6. Chen WX, Poon EK, Hutchins N, et al. Computational fluid dynamics study of common stent models inside idealised curved coronary arteries. *Comput Methods Biomech Biomed Engin* 2017; 20: 671–681.
7. Neidlin M, Corsini C, Sonntag SJ, et al. Hemodynamic analysis of outflow grafting positions of a ventricular assist device using closed-loop multiscale CFD simulations: preliminary results. *J Biomech* 2016; 49: 2718–2725.
8. Numata S, Itatani K, Kanda K, et al. Blood flow analysis of the aortic arch using computational fluid dynamics. *Eur J Cardiothorac Surg* 2016; 49: 1578–1585.
9. Gagnier JJ, Kienle G, Altman DG, et al. The CARE guidelines: consensus-based clinical case reporting guideline development. *Headache* 2013; 53: 1541–1547.
10. Cho YI and Kensey KR. Effects of the non-Newtonian viscosity of blood on flows in a diseased arterial vessel, part 1: steady flows. *Biorheology* 1991; 28: 241–262.
11. Liu B, Zheng J, Bach R, et al. Influence of model boundary conditions on blood flow patterns in a patient specific stenotic right coronary artery. *Biomed Eng Online* 2015; 14: S6.
12. Cheng C, Tempel D, Van Haperen R, et al. Atherosclerotic lesion size and vulnerability are determined by patterns of fluid shear stress. *Circulation* 2006; 113: 2744–2753.
13. Katranas SA, Kelekis AL, Antoniadis AP, et al. Differences in stress forces and geometry between left and right coronary artery: a pathophysiological aspect of atherosclerosis heterogeneity. *Hellenic J Cardiol* 2015; 56: 217–223.
14. Szostak J and Laurant P. The forgotten face of regular physical exercise: a ‘natural’ anti-atherogenic activity. *Clin Sci (Lond)* 2011; 121: 91–106.
15. Youssefi P, Gomez A, He T, et al. Patient-specific computational fluid dynamics—assessment of aortic hemodynamics in a spectrum of aortic valve pathologies. *J Thorac Cardiovasc Surg* 2017; 153: 8–20.e3.
16. Zhou X, Yin L, Xu L, et al. Non-periodicity of blood flow and its influence on wall shear stress in the carotid artery bifurcation: an in vivo measurement-based computational study. *J Biomech* 2020; 101: 109617.